ARTICLE

OBC
www.rsc.org/obc

Experimental and theoretical charge distribution in (*Z*)-*N*-methyl-*C*-phenylnitrone †

David E. Hibbs,*[a] Jane R. Hanrahan,[b] Michael B. Hursthouse,[c] David W. Knight,[d] Jacob Overgaard,[a] Peter Turner,[a] Ross O. Piltz[e] and Mark P. Waller[a]

[a] *School of Chemistry, University of Sydney, Sydney, NSW 2006, Australia. E-mail: d.hibbs@chem.usyd.edu.au; Fax: +61 (0) 2 9351 3329; Tel: +61 (0) 2 9036 9122*

[b] *Faculty of Pharmacy, University of Sydney, Sydney, NSW 2006, Australia. E-mail: sacjrh@med.usyd.edu.au; Fax: +61 (0) 2 9351 4391; Tel: +61 (0) 2 9351 2078*

[c] *School of Chemistry, University of Southampton, Highfield, Southampton, UK SO17 1BJ. E-mail: m.b.hursthouse@soton.ac.uk; Fax: +44 (0) 2380596723; Tel: +44 (0) 2380596722*

[d] *School of Chemistry, Cardiff University, P.O. Box 912, Cardiff, UK CF13TB. E-mail: knightdw@cf.ac.uk; Fax: +44 (0) 2924 874029; Tel: +44 (0) 2924 874000*

[e] *Neutron Scattering Section, Australian Nuclear Science and Technology Organisation, PMB 1, Menai, NSW 2234, Austalia. E-mail: rop@ansto.gov.au; Fax: +61(0) 2 9717 3606; Tel: +61 (0) 2 9717 3607*

Received 31st October 2002, Accepted 28th January 2003
First published as an Advance Article on the web 18th February 2003

The total experimental charge density in (*Z*)-*N*-methyl-*C*-phenylnitrone (**1**) has been determined using high-resolution X-ray diffraction data in combination with neutron diffraction data measured at 100 K in terms of the rigid pseudoatom model. Multipole refinement converged at $R = 0.03$ for 7163 reflections with $I > 2\sigma(I)$. Topological analysis of the total experimental charge density $\rho(r)$ and its Laplacian, $-\nabla^2\rho(r)$ and a comparison with high level theoretical gas-phase calculations reveals an unexpected electron distribution in the N–O group, both atoms having negative atomic charges, contrary to that commonly assumed in nitrone species. This observation is confirmed on examination of both the theoretical charges and the molecular electrostatic potential. Compound **1** contains a large number of hydrogen bonds and these are analysed using the atoms in molecules approach leading to quantitative values for bond strength, ranging from medium to very weak.

Introduction

Nitrones represent not only useful synthetic starting materials, widely used tools to detect free radicals, but also promising chemotherapeutic agents in cerebral ischemia and other pathologies as traps of biogenic oxygen-centred free radicals.[1] They effectively trap short-lived free radical species, to give nitroxide radicals, long-lived species that may be studied by electron spin resonance spectroscopy.[1] Nitrones occupy an important position in both heterocyclic and acyclic synthesis predominantly due to their ability to undergo thermally induced [1,3]-dipolar cycloadditions with a wide range of dipolarophiles, both in the inter- and intramolecular modes. Cleavage of the new N–O bond in the resulting oxazolidines leads to 1,3-aminoalcohols, usually in a stereoselective fashion, which can subsequently be converted into a wide range of targets.[1]

Less well exploited is the ability of nitrones to act as electrophiles, although some synthetically useful reactions of this type have been reported.[1] Our interest in this latter reactivity arose during exploratory work on reverse-Cope rearrangement reactions where suitable unsaturated hydroxylamines can be generated by the addition of allylamines, allylthiols and lithiated sulfones to a range of nitrones derived from aldehydes.[2] Our work has indicated that such nucleophilic additions show considerable differences to those displayed by corresponding aldehydes. Furthermore, predictions of the likely regio- and stereoselectivity of the ubiquitous [1,3] cycloaddition are more difficult to determine than other pericyclic processes, such as Diels–Alder reactions.[1–3] It was against this background that we undertook to determine the total experimental and theoretical charge density distribution $\rho(r)$, the Laplacian $-\nabla^2\rho(r)$, the molecular electrostatic potential and their relationship with chemical reactivity. We have clarified some outstanding inconsistencies in the intermolecular bonding descriptions of N^+–O^- and some distortions in the reactive surface predict likely centres of reactivity.

Experimental

X-Ray data collection and refinement

Crystals of **1** were grown from non-aqueous (EtOAc : hexane 1 : 1) solvents by slow evaporation. Single-crystal, high-resolution, low-temperature data were collected on a Bruker SMART 1000 CCD based diffractometer. Cell constants were obtained from the least squares refinement of 1863 reflections located between 5.7 and 119.2° 2θ. Three reciprocal space data shells were collected, with one sphere providing data between 2 and 58° 2θ, a second for data between 42 and 98° 2θ and a third for data between 72 and 128° 2θ. Data were collected at 100(2) K with ω-scan increments of 0.3°.

68156 reflections were integrated with the program SAINT+ [4] and merged with the program SORTAV.[5] 780 reflections were discarded as gross outliers, and the remaining 67466 reflections were corrected for absorption with an empirical absorption correction and averaged to give 11156 unique reflection with an average redundancy of 6.0. Only 177 reflections below $\sin(\theta)/\lambda$ of 1.24 Å^{-1} were missing, and only 463 reflections were measured once. The internal agreement of the data was 2.0%.

Neutron data collection and refinement

The single crystal neutron diffraction data was collected on the 2TANA four-circle diffractometer at the HIFAR reactor

† Electronic supplementary information (ESI) available: Tables of data. See http://www.rsc.org/suppdata/ob/b2/b210698a/

DOI: 10.1039/b210698a

located at Lucas Heights, Australia. The crystal was approx. 4 × 2.5 × 1.5 mm in dimensions and was mounted by wrapping it in aluminium foil and gluing the foil to an aluminium pin. The crystal was cooled to 100(2) K using the 2TANA helium closed cycle refrigerator. The intensities were collected and processed into integrated intensities using the ANSTO programs DIFF, DIFFPLOT and PEAKPOS. No significant trend was observed in the intensity of the two standard reflections, and so no time dependant correction was applied to the data. A total of 3990 independent reflections were measured over a 15 day period in three shells of increasing 2θ up to a maximum of 90°. The wavelength used was 1.235(1) Å. An analytical absorption correction was applied to the intensities, the correction varying from 0.48 to 0.68. Averaging equivalent and Friedel reflections gave 980 unique reflections with R(merge) = 6.9%, $R(\sigma)$ = 4.3%. $R1$ = 0.0311, $wR2$ = 0.0732; Full details of this refinement appear in the accompanying CIF.

Computational details

All gas phase DFT calculations were performed with the GAUSSIAN98 program package[6] at the 6-311++G** level of theory, using the three parameter hybrid exchange functional of Becke in combination with the gradient corrected exchange-correlation potential of Lee, Yang and Parr (B3LYP).[7] To analyse parts of the intermolecular hydrogen bonding pattern, a theoretical single point calculation was carried out at the same level of theory on a dimer of **1** in the experimental geometry. The AIMPAC suite of programs was used for the topological analysis of the theoretical wavefunctions.[8] All calculations were performed on a Silicon Graphics ORIGIN2400 computer [reference: http://www.ac3.com.au/sgi-origin-2400.htm]

Multipole refinement of the X-ray data

The structure of **1** (Fig. 1) was solved from direct methods using the program SHELXS.[9] To obtain unbiased positional and thermal parameters, an initial high-order independent atom model (IAM) refinement was carried out using only data with resolution better than 0.71 Å ($\sin(\theta)/\lambda > 0.7$ Å^{-1}). The hydrogen atoms were then moved to a distance corresponding to the X–H bond lengths obtained from the neutron diffraction study (see the Neutron data collection and refinement section) with freely refined isotropic displacement parameters. The atomic positions and anisotropic thermal displacement parameters for non-hydrogen atoms obtained from the high-angle refinement were kept fixed in the following refinements of the aspherical electron density using the Hansen–Coppens pseudoatom formalism.[10]

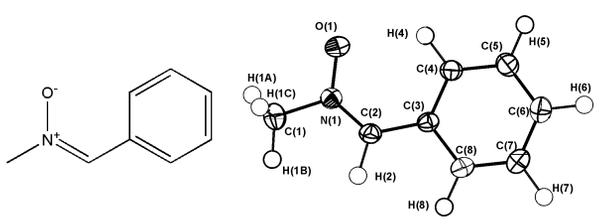

Fig. 1 ORTEP-drawing of **1** showing 80% probability ellipsoids.

In a crystal the electron density $\rho(r)$ can be described by a sum of aspherical pseudoatoms with nuclear positions $\{R_j\}$:

$$\rho(r) = \sum_j \rho_j(r - R_j)$$

With the pseudoatomic density form of:

$$\rho_j(r_j) = P_c\rho_c(r_j) + \kappa'^3 P_v\rho_v(\kappa' r_j) + \sum_{l=0}^{l_{max}} \sum_{m=0}^{l} \kappa''^3 P_{lm} R_l(\kappa'' r_j) d_{lmp}(\theta_j, \phi_j)$$

The expression for the pseudoatom density includes the usual spherical core, a term to describe the spherical component of the valence density, plus a deformation term describing the asphericity of the valence density. The radial functions $\{R_l(r_j)\}$ are modulated by angular functions $\{d_{lmp}(\theta_j,\phi_j)\}$, defined by axes centred on each atom. A number of radial functions may be used, the most common being Slater-type functions:

$$R_l(r) = Nr^{n_l} \exp(-\zeta_l r)$$

All refinements were performed with the least squares program XDLSM, part of the program package XD.[11] The atomic scattering factors were taken from International Tables of Crystallography,[12] and the radial functions were those of Clementi and Raimondi.[13]

First, a κ-refinement was performed.[14] In subsequent refinements the multipoles were included in separate steps, first dipoles (l_{max} = 1), then quadrupoles (l_{max} = 2) and finally octupoles (l_{max} = 3). In a final refinement, hexadecapoles (l_{max} = 4) were included for oxygen and nitrogen. Hydrogen atoms were treated with one monopole and the aspherical density was modeled by a single bond directed dipole. In all refinements the value of the Slater exponents (n_l) were the standard values of 2,2,2,3,4 (l = 0–4) for first row atoms, and 0,1 (l = 0–1) for hydrogen atoms. The values of ζ are given in the ESI.† The radial correction of the aspherical functions (κ'') was then refined with all other parameters kept fixed, before a final refinement of positions, thermal vibrations, and multipoles was performed. The refinements, in all of which only significant data on a $2\sigma(I)$ level were included, were considered to have reached convergence when the maximum shift was less than 10^{-3} of one su. Also, in all refinements, a non-crystallographic symmetry plane was imposed on the six carbon atoms multipole populations in the aromatic ring.

The final refinement gave an overall residual of $R_w(F^2)$ = 0.039, and the maximum residual density (+0.15 e Å^{-3}) is in the centre of the phenyl ring, as shown in Fig. 2. The average difference mean-squared displacement was 1.9 10^{-4} Å^2, indicating adequate de-convolution of thermal and electronic parameters.

The crystallographic details are listed in Table 1.

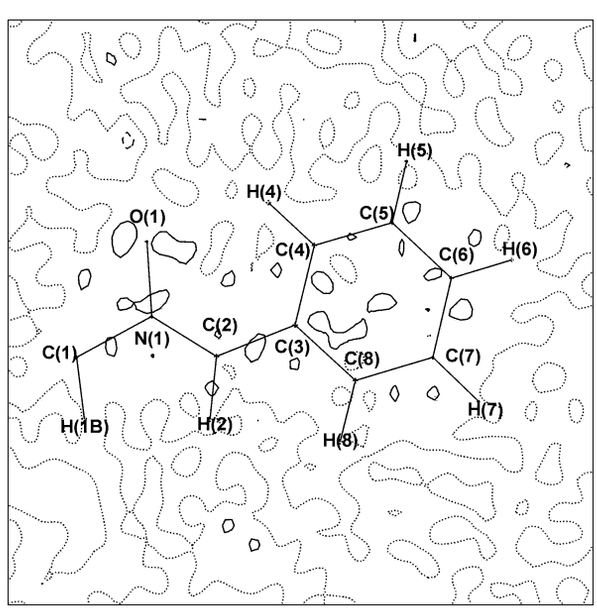

Fig. 2 Residual density in the molecular plane of **1**. The $\sin(\theta)/\lambda$-cutoff is 0.9 Å^{-1}. Solid lines show positive contours at an interval of 0.1 e Å^{-3}. Negative contours are shown by dashed lines. The zero contour is dotted.

Table 1 Crystallographic details

	X-ray	Neutron
Empirical formula	C_8H_9ON	
Formula weight/g mol^{-1}	1081.33	
Crystal system	Orthorhombic	
Space group	*Pbca*	
Z	8	
Temperature/K	100	
a/Å	9.5444(2)	9.544(2)
b/Å	7.7466(2)	7.756(2)
c/Å	19.1298(4)	19.106(4)
V/Å^3	1414.4(1)	1414.3(6)
ρ_{calc}/Mg m^{-3}	1.27	1.27
$F(000)$	576	576
μ/mm^{-1}	0.08	0.23
Crystal size/mm	0.25 × 0.20 × 0.20	4.0 × 2.5 × 1.5
λ/Å	0.7107	1.2355
$[\sin(\theta)/\lambda_{max}]$/Å^{-1}	1.241	0.572
Limiting indices (h; k, l)	0–23; 0–19; 0–47	−10,10; −8,8; −4,15
Number of collected reflections	71894	3990
Symmetry independent reflections	11156	980
Reflections with $I>2\sigma(I)$	7163	934
$100R_{int}$	0.020	0.069
$R(F)$	0.040	0.031
$R_w(F^2)$	0.039	0.073
S	1.70	1.18
Number of variables	240	173
N_{ref}/N_v	30.0	5.6

Table 2 Bond lengths (Å) and angles (°) in **1**

Bond	Experiment	Theory[a]
N(1)–O(1)	1.2912(4)	1.291
N(1)–C(1)	1.4711(4)	1.500
N(1)–C(2)	1.3096(4)	1.334
C(2)–C(3)	1.4524(4)	1.452
C(3)–C(4)	1.4073(4)	1.422
C(3)–C(8)	1.4085(4)	1.423
C(4)–C(5)	1.3950(4)	1.401
C(5)–C(6)	1.3941(5)	1.404
C(6)–C(7)	1.3974(5)	1.406
C(7)–C(8)	1.3914(5)	1.397
O(1)–N(1)–C(1)	114.66(3)	114.56
O(1)–N(1)–C(2)	125.53(3)	125.97
C(1)–N(1)–C(2)	119.81(3)	119.47
N(1)–C(2)–C(3)	126.28(3)	127.22
C(2)–C(3)–C(4)	125.44(3)	124.81
C(2)–C(3)–C(8)	115.63(3)	116.95
C(4)–C(3)–C(8)	118.91(3)	118.23
C(3)–C(4)–C(5)	119.88(3)	120.07
C(4)–C(5)–C(6)	120.73(3)	121.00
C(5)–C(6)–C(7)	119.76(3)	119.53
C(6)–C(7)–C(8)	119.93(3)	120.05
C(3)–C(8)–C(7)	120.74(3)	121.13

[a] Monomer optimsed at B3LYP/6-311++G** level of theory.

Table 3 Hydrogen bond geometries

Hydrogen bond	d_{1-2}/Å	d_{1-3}/Å	Angle/°
O(1) ··· H(4)–C(4)	2.196	2.8774(5)	119.0
O(1) ··· H(2)[a]–C(2)[a]	2.207	3.2577(5)	161.4
O(1) ··· H(1A)[b]–C(1)[b]	2.342	3.2365(5)	138.2
O(1) ··· H(8)[a]–C(8)[a]	2.507	3.4796(5)	148.6
C(3)[b] ··· H(5)–C(5)	2.884	3.6203(4)	125.2
C(8) ··· H(1C)[c]–C(1)[c]	2.909	3.6988(4)	129.3
C(4) ··· H(1B)[a]–C(1)[a]	2.888	3.9566(4)	169.8

[a] 0.5 + x, 0.5 − y, 1 − z, [b] 0.5 − x, −0.5 + y, z, [c] −x, −y, 1 − z.

Results and discussion

Geometric details

Structural details of compound **1** are listed in Table 2. The average difference in bond distances shows the correspondence between the theoretically optimised and the experimental structure. Based on the 10 bond distances (not including the hydrogens) this value is 0.011 Å, the largest discrepancies found in the non-aromatic part of the molecule. It is common to both geometries that the two bonds C(3)–C(4) and C(3)–C(8) are significantly longer than the other four C–C bonds in the phenyl-group.

There are a number of weak hydrogen bonds in the crystal structure of **1**. O(1) is involved in both intra- and intermolecular hydrogen bonding, participating in three C–H ··· O HBs. The only intramolecular HB (C(4)–H(4) ··· O(1)) in **1** is the shorter of all HBs (d(H ··· O) = 2.1959(4) Å), very similar in distance to the intermolecular HB C(2)–H(2) ··· O(1), d(H ··· O) = 2.2070(4) Å. However, the geometry of the HBs are different, see Table 3. The intramolecular HB has a very acute shape, whereas the intermolecular HBs are more perpendicular. However, only the intramolecular HB falls within the distance criterion suggested to be a prerequisite for the existence of a HB.[15] To fulfill this criterion, the C–O distance should be less than the sum of the oxygen and carbon van der Waals radii, which is 3.22 Å.[15]

Besides the C–H ··· O HBs, there are also a number of C–H ··· π interactions. One of the methyl hydrogens (H(1C)) is located above the midpoint of the aromatic ring of a neighbouring molecule, in an average distance to the six carbons of 3.06(15) Å and 2.70 Å above the mean-square plane of the six carbons. The shortest H–C distance (2.87 Å) is to C(7). In another C–H ··· π interaction, H(5) is located 2.57 Å above the mean-square plane of a nearby aromatic ring at an average distance from the carbons of 2.98(23) Å, with the closest carbon, C(8), only 2.69 Å away. The larger esd (0.23) for the C(5)–H(5) ··· π interaction than for C(1)–H(1C) ··· π (0.15 Å) quantifies that H(5) is more asymmetrically located above the neighbouring C_6 π-donor ring than is the case for the C(1)–H(1C) ··· π interaction.

Electron density

The electron density distribution (EDD) in **1** is illustrated by the static deformation density in the plane of the molecule in Fig. 3. This plot shows significant bonding electron density in all

Table 4 Topological analysis of **1**: first line experimental density, second line single point theory and third line theoretically optimised model. Only non-hydrogen atoms are included

A–B	ρ_{BCP}/e Å^{-3}	$\nabla^2\rho_{BCP}$/e Å^{-5}	ε	r_{A-B}/Å	r_{A-BCP}/Å	r_{B-BCP}/Å
N(1)–O(1)	3.00(2)	−3.32(8)	0.11	1.291	0.639	0.652
	2.82	−15.46	0.08	1.291	0.628	0.663
	2.80	−13.96	0.08	1.291	0.626	0.666
N(1)–C(1)	1.81(2)	−11.58(5)	0.08	1.471	0.867	0.604
	1.73	−15.85	0.07	1.471	0.907	0.564
	1.63	−13.41	0.08	1.500	0.888	0.612
N(1)–C(2)	2.56(2)	−26.77(9)	0.23	1.310	0.809	0.501
	2.30	−11.85	0.34	1.310	0.858	0.452
	2.19	−14.41	0.35	1.334	0.862	0.472
C(2)–C(3)	1.94(1)	−13.31(3)	0.15	1.453	0.758	0.694
	1.87	−17.25	0.14	1.452	0.750	0.703
	1.85	−16.21	0.15	1.452	0.745	0.708
C(3)–C(4)	2.14(1)	−16.00(3)	0.19	1.407	0.709	0.699
	2.03	−19.80	0.18	1.407	0.719	0.689
	1.96	−17.92	0.17	1.422	0.725	0.697
C(3)–C(8)	2.15(1)	−16.53(3)	0.20	1.409	0.705	0.704
	2.04	−19.96	0.19	1.408	0.708	0.700
	1.96	−17.94	0.18	1.423	0.716	0.708
C(4)–C(5)	2.20(1)	−17.33(3)	0.21	1.395	0.697	0.698
	2.08	−20.66	0.20	1.395	0.697	0.698
	2.04	−19.36	0.19	1.401	0.699	0.702
C(5)–C(6)	2.22(1)	−18.72(3)	0.17	1.394	0.695	0.700
	2.09	−20.88	0.19	1.394	0.695	0.699
	2.03	−19.23	0.19	1.404	0.700	0.704
C(6)–C(7)	2.21(1)	−17.37(3)	0.19	1.397	0.712	0.685
	2.07	−20.60	0.19	1.397	0.698	0.700
	2.02	−19.06	0.19	1.406	0.702	0.704
C(7)–C(8)	2.23(1)	−17.58(3)	0.23	1.391	0.679	0.712
	2.09	−20.85	0.21	1.391	0.691	0.701
	2.05	−19.56	0.21	1.397	0.695	0.702

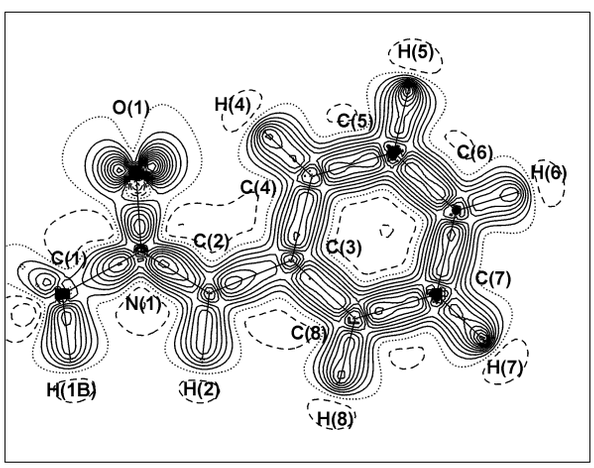

Fig. 3 Static deformation density. Contour levels as in Fig. 2.

the bonds, as well as two well-separated lone pairs on the oxygen atom in the plane of the molecule. The clear localisation of these lone pairs confirms that O(1) is in a sp^2-hybridised state, forming a nominal double bond with N(1).

Topological analysis

Based on the theory of atoms in molecules (AIM),[8] we have performed a topological analysis of the total electron density described by the refined multipoles. The topological analysis locates the critical points (CPs) in the electron density distribution. As a subset of the CPs, the bond critical points (BCPs) are a necessary and sufficient prerequisite for the existence of a chemical bond between two atoms. The analysis of the EDD in the BCPs gives important information of the nature of interatomic interaction. In particular, a topological analysis leads to quantities for the intra- and intermolecular interaction that can be compared to theory. The topological parameters for the BCPs in **1** involving only non-hydrogen atoms are collected in Table 4, showing both the experimental and the theoretical values.

The completeness of the modelling of the EDD can be checked by considering the Morse equation, which requires that a special relationship (#nuclei − #BCP + #RCP − #CCP = 0) has to be fulfilled.[16] In **1**, the number of nuclei is 19, the number of BCPs within the molecule is 20, the number of intermolecular hydrogen bonds is 6, and the number of ring critical points (RCPs) is 7, while the number of cage critical points (CCPs) is zero, thus the Morse equation is obeyed.

Several features in Table 4 deserve mentioning. First of all, there is a large discrepancy between the experimental and theoretical value for the Laplacian of the electron density in the N–O bond. The experiment gives a much less negative value, while at the same time a higher value of ρ_{BCP} is observed. In the AIM theory, a covalent or open-shell interaction is characterised by a negative value of $\nabla^2\rho_{BCP}$, while an electrostatic or closed-shell interaction is identified by a positive value of $\nabla^2\rho_{BCP}$. The designation of either open or closed-shell interaction to a bond may demand a more extensive description of the bond than merely an evaluation of one or two properties in one point. Fig. 4 depicts the Laplacian of the experimental density, again in the molecular plane. This picture shows a gap between the nitrogen and oxygen, which has also been observed, but not commented upon, in other EDD studies of N–O bond containing structures.[17] However, the theoretical density shows a clear overlap between the two valence shell charge concentrations (VSCCs) of nitrogen and oxygen, indicative of an open-shell interaction, see Fig. 5. This bond clearly has a polar and partly not-shared interaction, in-line with the proposed N^+–O^- configuration. However, examination of the atomic charges of N(1) and O(1) reveal surprisingly that this is not the case. For N(1) the monopole (P_v) charge is −0.30(4) e, while P_v for O(1) is −0.47(2) e, indeed, support for this is seen from the integrated atomic charges taken from the single point gas-phase calculations where N(1) and O(1) have charges of −0.53 e, and −0.57 e respectively. From Table 4 it is also clear that the experimental values for ρ_{BCP} are consistently higher

Table 5 Lone pair (LP) (3,−3) critical point data for (**1**)

Multipole refined				B3LYP/6-311++G**		
Lone Pair	ρ	$\nabla^2\rho$	d^a	ρ	$\nabla^2\rho$	d^a
LP1	6.54	−138.99	0.337	6.61	−134.03	0.338
LP2	6.71	−146.86	0.338	6.61	133.56	0.339

[a] Distance from oxygen nucleus to LP centroid (Å)

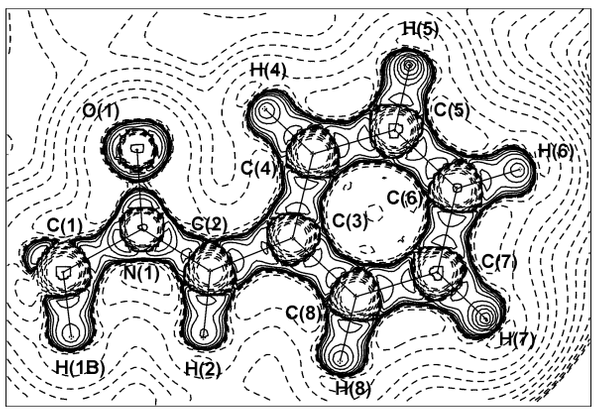

Fig. 4 Experimental negative Laplacian of the electron density in the same plane as in Fig. 3. Positive contours are shown by solid lines, negative contours with dashed lines. The zero contour is dotted. Contour intervals are $\pm 2, 4, 8 \times 10^n$, $n = -3, -2, -1, 0, 1, 2$ [e Å^{-5}].

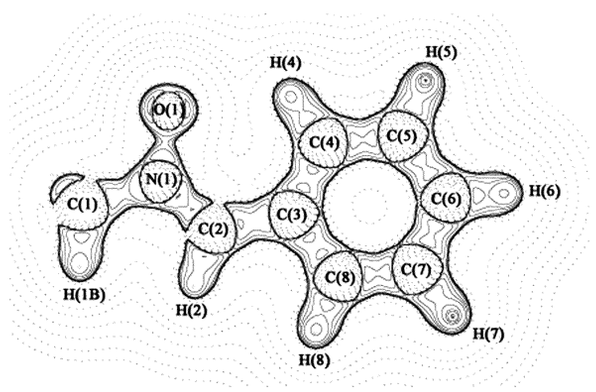

Fig. 5 Theoretical negative Laplacian of the electron density in the same plane as in Fig. 4. Contours are as in Fig. 4.

than the theoretical ones, while the bond distances are all shorter. We have no explanation for this systematic discrepancy between the bond distances in the experimental *vs*. the theoretical structures. Changes in unit cell parameters, which would have a significant impact on the bond distances, were determined carefully from a large number of reflections and is therefore not a likely reason for the discrepancy.

The values of the topology of the oxygen lone pairs (LPs) are given in Table 5 (LP1 is *syn*, LP2 *anti* to the methyl group). Here we see that the agreement between the experimentally determined vales of ρ and those from theory is excellent, with a maximum discrepancy of 0.1 e Å^{-3}. Despite the almost identical radial distances (differing by only 0.001 Å) of the oxygen lone pairs, the values of the Laplacian are quite different, and this is almost certainly due to the effects of hydrogen bonding.

Theoretical calculations allow us to calculate the covalent bond order directly (at the experimental geometry), using the method proposed by Ángyán.[18] These show bond orders of *ca.* 1.5 for O(1)–N(1), slightly less than unity (0.9) for C(1)–N(1), 1.3 for N(1)–C(2), 1.1 for C(2)–C(3), while the aromatic C–C bonds have an average value of 1.37. Average values for C(sp^3)–H and C(sp^2)–H are 0.92 and 0.83 respectively. This lends credence to the observation that O(1) has a considerable amount of sp^2 character as mentioned earlier. The value for the C=N double bond (1.3), also supports experimental observations that this bond has enhanced electrophilicity with respect to imines and other azomethines.[1]

Hydrogen bonding and the charge distribution

As mentioned above, the crystal structure of **1** contains a number of weak hydrogen bonds. Each of the four C–H ⋯ O(1) interactions give rise to bond critical points in the electron density (Table 6). The difference between ρ_{BCP} is striking in the two HBs to H(4) and to H(2). From their hydrogen bond distances, no distinction is apparent between these two HBs, but the geometry suggests that the intramolecular HB is too far away from optimal HB geometry to have any significant strength.[15] However, adopting the value of ρ_{BCP} as a measure of HB strength then it is exactly this strained HB that is the stronger (Table 6).

Even weaker hydrogen bonds are found as C–H ⋯ π interactions. As mentioned in the Geometry details section, the aromatic ring in **1** is involved in C–H ⋯ π interactions to symmetry related molecules on both sides. After extensive searching, we have only been able to locate one BCP in both of these interactions. In the C(1)–H(1C) ⋯ π interaction, the BCP connects H(1C) to both C(8) and C(3), which are 1.793 Å and 1.886 Å away from the BCP, respectively, while the H(1C)–BCP–C angles are 145.1° and 169.2°, to C(8) and C(3). No BCP could be located between H(1C) and the closest carbon, C(7). In the other C–H ⋯ π interaction, a similar situation could be recognised. No BCP was found between H(5) and C(8). Instead, the only BCP is found almost exactly on the line between H(5) and C(3), the angle H(5)–BCP–C(3) being 175.0°. A representative experimental Laplacian map for the intramolecular hydrogen bond is given in Fig. 6.

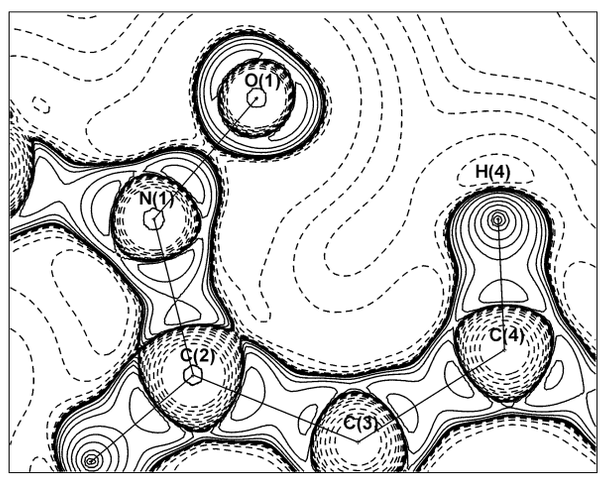

Fig. 6 O(1) ⋯ H(4)–C(4) hydrogen bond. Contours as in Fig. 4.

It is interesting to examine the bond paths for the two intermolecular hydrogen bonds from O(1) to H(2) and H(8), see Fig. 7. The path from O(1) to the BCPs follow a curve inwards and the two BCPs are not very far from the ring critical point (RCP) that must by definition exist and is found in between the two BCPs. The difference between the lengths of the bond paths and the straight interatomic lines are 0.052 Å for O(1) ⋯ H(2) and 0.122 Å for O(1) ⋯ H(8). The distances from the BCPs to the RCP are 0.77 Å (O(1) ⋯ H(2)) and 0.31 Å (O(1) ⋯ H(8)). The proximity of the RCP and in particular the O(1) ⋯ H(8) BCP seems to indicate the existence of instability in the system, as the coalescence of a BCP and a RCP leads to a singularity in the electron density $\rho(r)$ and an unstable structure.[8]

As mentioned above, the electron density suggests that the intramolecular HB between O(1) and H(4) is the stronger of all HBs found in the crystal structure. This may be due to the fact that H(4) experiences a maximum overlap with an electron lone

Table 6 Topological analysis of the hydrogen bonds in **1**

Hydrogen bond	Model	ρ_{BCP}/e Å^{-3}	$\nabla^2\rho_{BCP}$/e Å^{-5}	ε	d_{A-B}/Å	r_{A-BCP}/Å	r_{B-BCP}/Å
O(1) ··· H(4)–C(4)	Exp	0.108(1)	1.83(1)	0.20	2.221	1.308	0.913
	Calc	0.129	1.69	0.07			
O(1) ··· H(2)[a]–C(2)[a]	Exp	0.056(2)	1.50(1)	0.22	2.235	1.385	0.850
	Calc	0.101	1.23	0.11			
O(1) ··· H(1A)[b]–C(1)[b]	Exp	0.054(1)	1.03(1)	0.23	2.377	1.400	0.978
	Calc	—	—	—			
O(1) ··· H(8)[a]–C(8)[a]	Exp	0.030(1)	0.71(1)	0.12	2.572	1.536	1.037
	Calc	0.064	0.67	0.11			
C(3)[b] ··· H(5)–C(5)	Exp	0.031(1)	0.49(1)	1.00	2.887	1.749	1.138
	Calc	—	—	—			
C(8) ··· H(1C)[c]–C(1)[c]	Exp	0.027(1)	0.39(1)	1.82	3.044	1.793	1.251
	Calc	—	—	—			
C(4) ··· H(1B)[a]–C(1)[a]	Exp	0.011(1)	0.43(1)	1.41	2.908	1.877	1.030
	Calc	0.035	0.37	0.63			

[a] 0.5 + x, 0.5 − y, 1 − z, [b] 0.5 − x, −0.5 + y, z, [c] −x, −y, 1 − z.

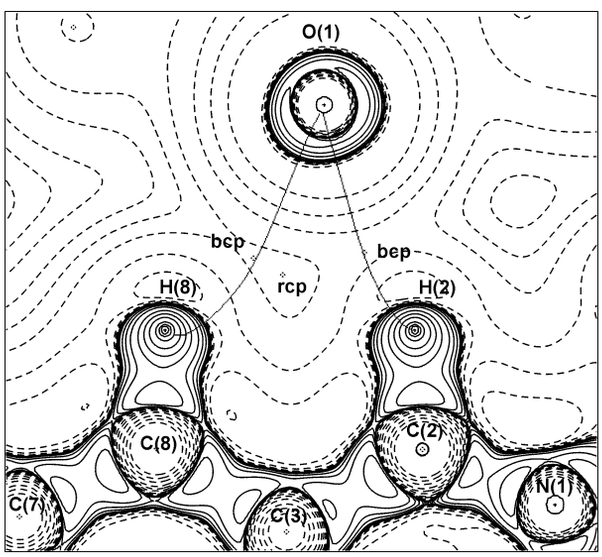

Fig. 7 Experimental bond paths for the intermolecular HBs displayed on experimental Laplacian map. Contours as in Fig. 4.

pair on the HB acceptor atom, O(1). To examine this, the lone pairs on O(1) were located in a search for maxima in the Laplacian of the density in a shell close to the oxygen.[8] The hydrogen bond directionality[19] can be quantified as the angle O(1)–LP–H, where LP is the oxygen lone pair and H is the hydrogen, involved in the HB. This angle is 176.9° in the O(1) ··· H(4) HB, while it is much lower for the C(2)–H(2)–O(1) HB (96.3°), showing the much lower overlap for the latter HB.

From the theoretical calculations on the dimer of **1** the LPs are found such that $\psi_1 + \psi_2 + \theta = 358.0°$ (for a definition of the angles, see Fig. 8) for the oxygen modelled with hydrogen bonds, while for the single molecule calculation with the corresponding 'free' oxygen that value is exactly 360°, *.i.e.* completely in the plane. Turning now to the experimental LP positions, it seems that inter- and intra-molecular hydrogen bonding has a very similar effect on the angular positions of the oxygen LPs, where $\psi_1 + \psi_2 + \theta = 358.3°$. The angular positions of the LPs show between a 3–7° discrepancy from the theoretical value, but nonetheless are realistic for a carbonyl type oxygen.

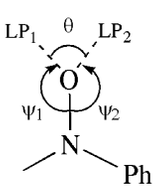

Fig. 8 Schematic drawing of the lone pair position on O(1).

Table 7 Energy densities in the HBs in **1**. G, V, H are given in hartrees and G/ρ in hartree Å

Hydrogen bond	G	V	H	G/ρ
O(1) ··· H(4)–C(4)	0.10	−0.08	0.02	0.97
O(1) ··· H(2)[a]–C(2)[a]	0.08	−0.05	0.03	1.37
O(1) ··· H(1A)[b]–C(1)[b]	0.05	−0.04	0.02	1.00
O(1) ··· H(8)[a]–C(8)[a]	0.04	−0.02	0.01	1.17
C(3)[b] ··· H(5)–C(5)	0.03	−0.02	0.01	0.81
C(8) ··· H(1C)[c]–C(1)[c]	0.02	−0.01	0.01	0.74
C(4) ··· H(1B)[a]–C(1)[a]	0.02	−0.01	0.01	1.87

[a] 0.5 + x, 0.5 − y, 1 − z. [b] 0.5 − x, −0.5 + y, z. [c] −x, −y, 1 − z .

The HBs are mainly electrostatic interactions, thus the energy density within these bonds can be easily calculated from the topological parameters describing these interactions with the approximation suggested by Abramov:[20]

$$G(r) = \frac{3}{10}(3\pi^2)^{2/3}\rho(r)^{5/3} + \frac{1}{72}[\nabla^2\rho(r)]^2/\rho(r) + \frac{1}{6}\nabla^2\rho(r)$$

The energy densities have been correlated to the bond energies in HBs by Espinosa *et al.*,[21] and the results confirm the O(1) ··· H(4) HB being the strongest (Table 7).

Electrostatic potential

The molecular electrostatic potential (MEP) can be calculated for the isolated molecule of **1** as it appears in the crystalline state. Thus, it includes in principle all the contributions of polarisation, electron correlation and charge transfer effects. It should be noted that no charge transfer has been allowed between molecules, which are fixed as neutral. Fig. 9a shows the theoretical MEP (taken from the dimer calculation) as negative (purple) and positive (blue) regions of this property at the ±0.30 e Å^{-1} isosurface value. Fig. 9b shows the experimental values as both negative (purple: −0.3 e Å^{-1}) and positive (blue: 0.3 e Å^{-1}) regions of the MEP. It is quite clear that the negative potential is concentrated around O(1), while the rest of the molecule has a positive electrostatic potential. It is important to note the asymmetry of the negative electrostatic potential observed near O(1) in the theoretical MEP. This observation can be attributed to O(1)'s involvement in hydrogen bonding, with hydrogen bond strength decreasing as the negative MEP is polarized right to left. When compared to the experimental MEP this effect is even more apparent as this includes hydrogen bonding motifs that were not modeled in the gas phase calculation.

Intermolecular interaction energies

It has recently been shown that intermolecular energies calculated from the set of refined multipoles result in accurate

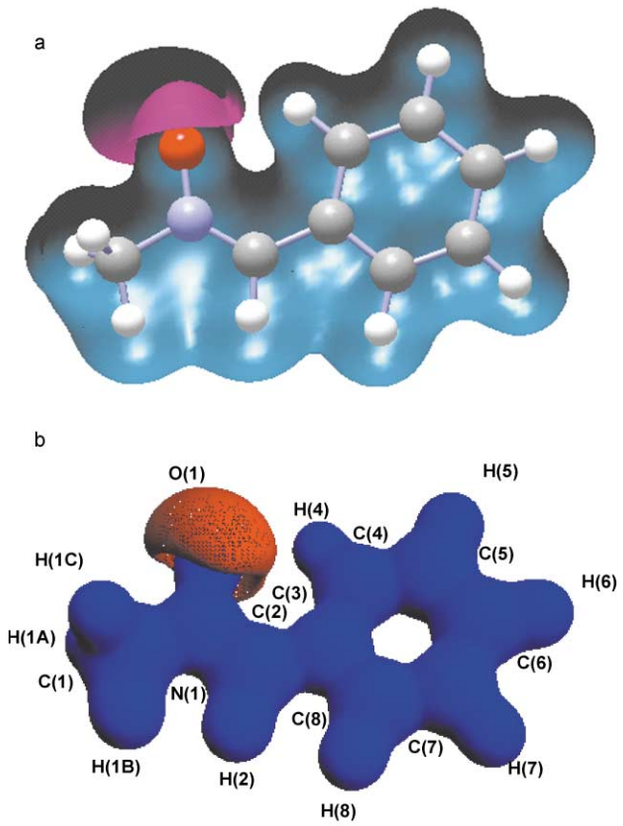

Fig. 9 (a) Theoretical electrostatic potential (from the dimer) in **1**. The potential of +0.3 e Å^{-1} is shown by the blue isosurface, the purple isosurface shows the −0.3 e Å^{-1}-level, (b) Experimental electrostatic potential in **1**. The potential of +0.3 e Å^{-1} is shown by the blue isosurface, the purple isosurface shows the −0.3 e Å^{-1}-level,

estimates of crystal lattice energies.[22] Using this experimental charge density approach leads to a lattice energy of −51.6 (21) kJ mol^{-1} in **1**. The contributing terms are the electrostatic, exchange/repulsion and dispersion energies, which are −83.9, 172.2 and −139.9 kJ mol^{-1}, respectively. For comparison, the lattice energy in the *p*-nitroaniline crystal[22] is −96.5(114) kJ mol^{-1}, with a dominant contribution from the dispersion term, as is the situation for **1**. The lattice energy for **1** is relatively small, suggesting a rather loose crystal packing. This is in full accord with the low value observed for the dipole moment (4.9 D).

Conclusions

We have determined the high-resolution electron distribution of (*Z*)–*N*-methyl-*C*-phenylnitrone based upon the standard multipole formalism, and compared the results throughout with analogous theoretical calculations. These studies indicate that the gross structural details alone do not give a clear picture of the chemical bonding present, rather it is the topological properties of the electron density that accurately reveal the nature of these bonds. It is to be noted that the lack of an *m*-symmetry constraint on the planar C=N–O group reveals a considerable amount of electron delocalisation over this region, and hence to a formally sp^2 hybridised O, complete with localised lone pairs. This is particularly evident in the Laplacian, and the polarisation of the molecular electrostatic potential, the former indicating the potential of nitrones to act as nucleophiles, while the latter revealing the possibility of nitrones acting as electrophiles, as has indeed been exploited synthetically. It has been shown that careful experimental charge density studies can reveal a great deal of knowledge regarding the chemical bonding introduced by weak hydrogen bonding, and how the values determined at the critical points can be correlated with hydrogen bond strength. We believe that the ability for charge density studies to shed light on weak intermolecular interactions is of fundamental importance in crystallography.

Acknowledgements

We would like to thank the Australian Research Council and the Danish Research Council (JO) for funding this work, the Australian Centre for Advanced Computing and Communications (ac3) [http://www.ac3.com.au] for a generous allocation of computer resources. DEH would also like to thank the Royal Society of Chemistry for a Journals Grant.

References

1 For reviews see R. Grigg, *Chem. Soc. Rev.*, 1987, **16**, 89; M. Lombardo and C. Trombini, *Synthesis*, 2000, 759–774.
2 A. R. Wheildon, D. W. Knight and M. P. Leese, *Tetrahedron Lett.*, 1997, **38**, 8553.
3 A. Padwa, *Comp. Org. Synth.*, 1991, **4**, 1069; R. Sustmann, *Heterocycles*, 1995, **40**, 1.
4 Bruker, SMART, SAINT+ and XPREP. Area detector control, data integration and reduction software. Bruker Analytical X-ray Instruments Inc., Madison, Wisconsin, USA, 1995.
5 R. H. Blesssing, *J. Appl. Crystallogr.*, 1989, **22**, 396.
6 M. J. Frisch, G. W. Trucks, H. B. Schlegel, G. E. Scuseria, M. A. Robb, J. R. Cheeseman, V. G. Zakrzewski, J. A. Montgomery, Jr., R. E. Stratmann, J. C. Burant, S. Dapprich, J. M. Millam, A. D. Daniels, K. N. Kudin, M. C. Strain, O. Farkas, J. Tomasi, V. Barone, M. Cossi, R. Cammi, B. Mennucci, C. Pomelli, C. Adamo, S. Clifford J. Ochterski, G. A. Petersson, P. Y. Ayala, Q. Cui, K. Morokuma, D. K. Malick, A. D. Rabuck, K. Raghavachari, J. B. Foresman, J. Cioslowski, J. V. Ortiz, A. G. Baboul, B. B. Stefanov, G. Liu, A. Liashenko, P. Piskorz, I. Komaromi, R. Gomperts, R. L. Martin, D. J. Fox, T. Keith, M. A. Al-Laham, C. Y. Peng, A. Nanayakkara, C. Gonzalez, M. Challacombe, P. M. W. Gill, B. Johnson, W. Chen, M. W. Wong, J. L. Andres, C. Gonzalez, M. Head-Gordon, E. S. Replogle, J. A. Pople, *Gaussian 98, Revision A. 7*, Gaussian, Inc., Pittsburgh PA, 1998.
7 (*a*) A. D. Becke, *J. Chem. Phys.*, 1993, **98**, 5648; (*b*) C. Lee, W. Yang and R. G. Parr, *Phys. Rev. B*, 1988, **38**, 3098; (*c*) P. J. Stevens, F. J. Devlin, C. F. Chabalowski and M. J. Frisch, *J. Phys. Chem.*, 1994, **98**, 11623; (*d*) C. Adamo and V. Barone, *Chem. Phys. Lett.*, 1997, **274**, 242.
8 R. F. W. Bader, *Atoms in Molecules a Quantum Theory*, Clarendon Press, Oxford, 1990.
9 G. M. Sheldrick, SHELX-86. Program for crystal structure refinement, University of Göttingen, Germany 1986.
10 N. K. Hansen and P. Coppens, *Acta Crystallogr. Sect. A.*, 1979, **39**, 909–921.
11 T. Kortisanszky, S. T. Howard, P. R. Mallinson, Z. Su, T. Richter and N. K. Hansen, XD—a computer program package for the multipole refinement and analysis of electron densities from diffrraction data.Free University of Berlin, 1997.
12 *International Tables of Crystallography, Vol. C*, ed. A. J. C. Wilson, Kluwer Academic Publishers, Dordrecht, 1992, pp. 500–502, 219–222, 193–199.
13 E. Clementi and D. L. Raimondi, *J. Chem. Phys.*, 1963, **38**, 2686–2689.
14 P. Coppens, X-ray Charge Densities and Chemical Bonding, Oxford University Press, 1997.
15 F. Hibbert and J. Emsley, *Adv. Phys. Org. Chem.*, 1990, 255–379.
16 C. K. Johnson, *ACA Abstracts Ser. 2*, 1992, **29**, 105.
17 E. A. Zhurova, A. Martin and A. A. Pinkerton, *J. Am. Chem. Soc.*, 2002, **124**, 8741–8750.
18 J. G. Ángyán, E. Rosta and P. R. Surján, *Chem. Phys. Lett.*, 1999, **299**, 1–8.
19 T. W. Hambley, D. E. Hibbs, P. Turner, S. T. Howard and M. B. Hursthouse, *J. Chem. Soc., Perkin Trans. 2*, 2002, **2**, 235–239.
20 Yu. A. Abramov, *Acta Crystallogr. Sect. A*, 1997, **53**, 264–272.
21 E. Espinosa, E. Molins and C. Lecomte, *Chem. Phys. Lett.*, 1998, **285**, 170–173.
22 Yu. A. Abramov, A. Volkov, G. Wu and P. Coppens, *Acta Crystallogr. Sect. A*, 2000, **56**, 585–591.